New Phytologist

# ER body-resident myrosinases and tryptophan specialized metabolism modulate root microbiota assembly

Arpan Kumar Basak[1,2,3], Anna Piasecka[4], Jana Hucklenbroich[3], Gözde Merve Türksoy[3], Rui Guan[3], Pengfan Zhang[3], Felix Getzke[3], Ruben Garrido-Oter[3,5], Stephane Hacquard[3,5], Kazimierz Strzałka[2,6], Paweł Bednarek[4], Kenji Yamada[2] and Ryohei Thomas Nakano[3,7]

[1]Institute of Environmental Sciences, Faculty of Biology, Jagiellonian University, Krakow, 30-387, Poland; [2]Malopolska Centre of Biotechnology, Jagiellonian University, Krakow, 30-387, Poland; [3]Department of Plant Microbe Interactions, Max Planck Institute for Plant Breeding Research, Cologne, 50829, Germany; [4]Institute of Bioorganic Chemistry, Polish Academy of Sciences, Poznan, 61-704, Poland; [5]Cluster of Excellence on Plant Sciences (CEPLAS), Max Planck Institute for Plant Breeding Research, Cologne, 50829, Germany; [6]Faculty of Biochemistry, Biophysics and Biotechnology, Department of Plant Physiology and Biochemistry, Jagiellonian University, Krakow, 30-387, Poland; [7]Present address: Faculty of Science, Hokkaido University, Sapporo, 060-0810, Japan

Author for correspondence:
*Ryohei Thomas Nakano*
Email: *rtnakano@sci.hokudai.ac.jp*

## Summary

• Endoplasmic reticulum (ER) bodies are ER-derived structures that contain a large amount of PYK10 myrosinase, which hydrolyzes tryptophan (Trp)-derived indole glucosinolates (IGs). Given the well-described role of IGs in root–microbe interactions, we hypothesized that ER bodies in roots are important for interaction with soil-borne microbes at the root–soil interface.

• We used mutants impaired in ER bodies (*nai1*), ER body-resident myrosinases (*pyk10bglu21*), IG biosynthesis (*myb34/51/122*), and Trp specialized metabolism (*cyp79b2b3*) to profile their root microbiota community in natural soil, evaluate the impact of axenically collected root exudates on soil or synthetic microbial communities, and test their response to fungal endophytes in a mono-association setup.

• Tested mutants exhibited altered bacterial and fungal communities in rhizoplane and endosphere, respectively. Natural soils and bacterial synthetic communities treated with mutant root exudates exhibited distinctive microbial profiles from those treated with wild-type (WT) exudates. Most tested endophytes severely restricted the growth of *cyp79b2b3*, a part of which also impaired the growth of *pyk10bglu21*.

• Our results suggest that root ER bodies and their resident myrosinases modulate the profile of root-secreted metabolites and thereby influence root–microbiota interactions.

## Introduction

Endoplasmic reticulum (ER) bodies (Fig. 1a; Matsushima *et al.*, 2003a) are ER-derived spindle-shaped organelles observed in plants from a monophyletic group of families within the order Brassicales, that is, Brassicaceae, Cleomaceae, and Capparaceae (Hayashi *et al.*, 2001; Hara-Nishimura & Matsushima, 2003). These structures were originally discovered in radish roots using an electron microscope and named 'dilated cisternae' after their characteristics as a part of the ER cisternae (Bonnett & Newcomb, 1965). ER bodies are constitutively developed in the ground tissue of roots (epidermis, cortex, and endodermis), implying their role in root physiology. In aboveground tissues, ER bodies are found mainly in seedlings (cotyledon and hypocotyl), especially in the epidermal cell layers, but not in mature tissues, such as mesophyll cells and rosette leaves. Interestingly, ER body formation is strongly induced by wounding or jasmonic acid treatment in mature rosette leaves (Matsushima *et al.*, 2002;

Ogasawara *et al.*, 2009), suggesting a role in wounding stress response. Consistently, recent studies showed that leaf ER bodies are important for defense against herbivory (Nakazaki *et al.*, 2019; Yamada *et al.*, 2020). Another study suggested that leaf ER bodies triggered by a pathogen-derived jasmonate mimicry, coronatine, negatively regulate immune responses against a bacterial pathogen *Pseudomonas syringae* pv tomato DC3000 (Rufian *et al.*, 2021). These findings suggest that leaf ER bodies are involved in environmental interactions, while the role of root ER bodies remains ununderstood.

ER body formation in leaves and roots is regulated by a transcription factor NAI1 in *Arabidopsis thaliana*, and β-glucosidases, namely PYK10 and BGLU21 in roots/seedlings and BGLU18 in rosette leaves, are accumulated inside the ER bodies (Matsushima *et al.*, 2003b; Ogasawara *et al.*, 2009). These enzymes were recently shown to be myrosinases (Nakano *et al.*, 2017; Nakazaki *et al.*, 2019), which is a class of β-glucosidases that are capable of hydrolyzing sulfur-containing specialized
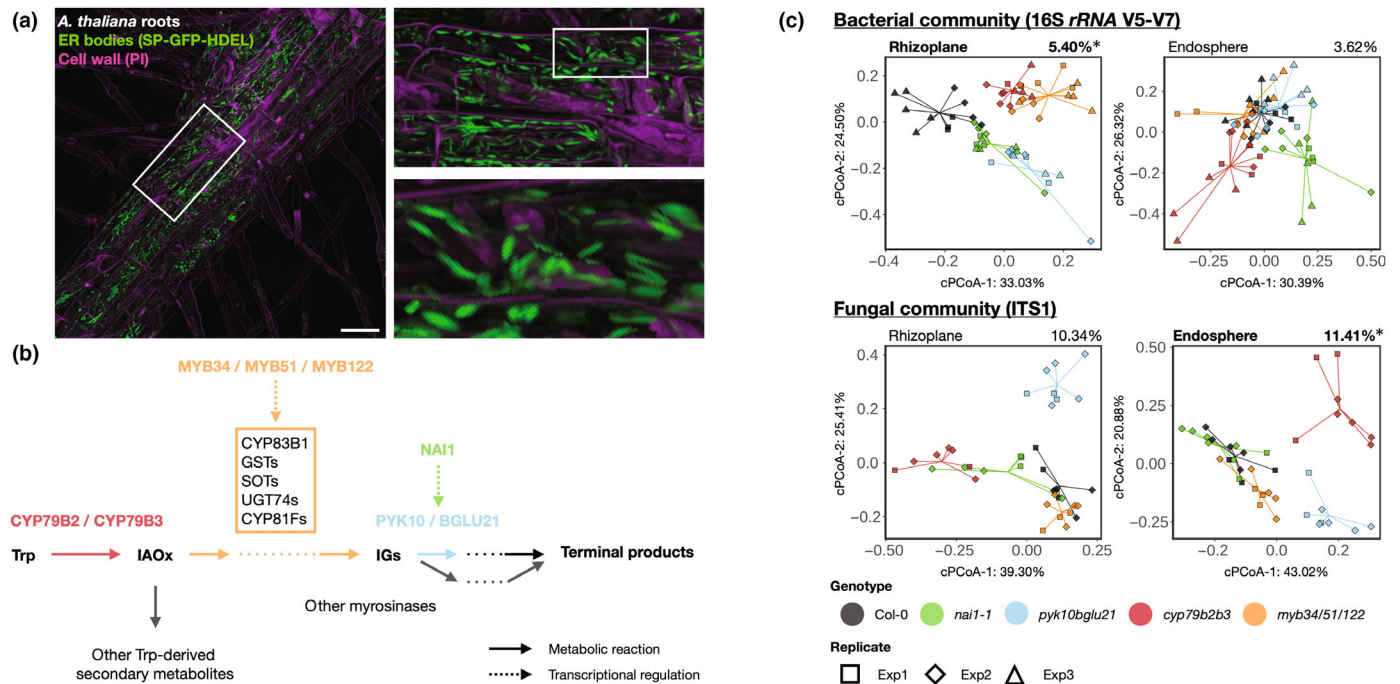
Fig. 1 Endoplasmic reticulum (ER) bodies and Trp metabolism play a role in root-associated microbiota assembly. (a) Roots of *Arabidopsis thaliana* developing a large amount of ER bodies, visualized by ER-localized GFP (SP-GFP-HDEL). Cell wall was stained by propidium iodide. The bar corresponds to 50 µm. (b) Representation of IG biosynthetic and catabolic pathways. Arrows and dotted arrows indicate metabolic reactions and transcriptional regulation, respectively. (c) Constrained principal coordinates analysis (cPCoA) of the bacterial and fungal community structures in the roots of Col-0 as well as mutants impaired in ER body formation (*nai1-1*), ER body-resident myrosinases (*pyk10bglu21*), IG biosynthesis (*myb34/51/122*) and Trp metabolism (*cyp79b2b3*) based on Bray–Curtis dissimilarities. Ordination was constrained by genotypes and conditions by soil batches, biological replicates, and sequencing runs. Colors and shapes represent the genotypes and biological replicates, respectively. Variation explained by genotypes based on permutational analyses of variance (PERMANOVA; $n = 1000$) is indicated at the top right, and asterisks indicate its statistical significance ($\alpha = 0.05$). GST, glutathione-*S*-transferase; IAOx, indole-3-acetaldoxime; IG, indole glucosinolates; SOT, sulfotransferase; Trp, tryptophan; UGT, uridine diphosphate-glycosyltransferase.

thio-glucosides called glucosinolates. Glucosinolates accumulate in plants of the order Brassicales and are crucial for defense against herbivores and microbial pathogens (Wittstock & Halkier, 2002). While intact glucosinolates are biologically inert, their hydrolysis by myrosinases removes the glucose moiety and produces unstable aglycons that decompose into a wide range of terminal products, such as isothiocyanates and nitriles, which are thought to be actively influencing the behavior of insects and microbes. It is, therefore, conceivable that the terminal products of glucosinolate catabolism initiated by these ER body-resident myrosinases mediate the defensive role of ER bodies against the woodlice.

Glucosinolates are categorized into several groups based on the side chain structures. Glucosinolates with an aliphatic side chain (aliphatic glucosinolates, AGs) and with a benzyl side chain (benzyl glucosinolates; BGs; also known as aromatic glucosinolates) are mainly produced from methionine (Met) and phenylalanine (Phe), respectively, while glucosinolates with an indolic side chain (indole glucosinolates, IGs) are primarily produced from tryptophan (Trp). These glucosinolates and their catabolic products are well known for their role in antiherbivorous defense in leaves and seeds, as well as in defense against microbial pathogens. For instance, genetic disruption of leaf IG metabolism results in severe disease susceptibility to a wide range of

filamentous pathogens (Bednarek *et al.*, 2009; Clay *et al.*, 2009; Hiruma *et al.*, 2010; Frerigmann *et al.*, 2016). Furthermore, genetic disruption of CYTOCHROME P450 (CYP) 79B2 and 79B3 enzymes, which are responsible for the production of all Trp-derived specialized metabolites including IGs, triggers aberrant interaction with soil-borne nonpathogenic microbes at the root–soil interface (Lahrmann *et al.*, 2015; Hiruma *et al.*, 2016; Koprivova *et al.*, 2019; Frerigmann *et al.*, 2021; Wolinska *et al.*, 2021). For example, this mutant cannot properly manage the accommodation of beneficial endophytic fungi, such as *Serendipita vermifera*, *Serendipita indica*, and *Colletotrichum tofieldiae*, and exhibits severe growth defects in the presence of these fungi (Lahrmann *et al.*, 2015; Hiruma *et al.*, 2016). Likewise, the *cyp79b2b3* mutant in the presence of a synthetic microbial community (SynCom) composed of commensal bacteria and endophytic fungi fails to control the overall abundance of fungi in roots ('fungal load'), and its growth is strongly restricted (Wolinska *et al.*, 2021).

Notably, Trp-derived specialized metabolites, including IG catabolites, are reported to be secreted into the rhizosphere (Schreiner *et al.*, 2011; Strehmel *et al.*, 2014; Xu *et al.*, 2017). *A. thaliana* roots express several myrosinases, including but not limited to PYK10 and BGLU21. Namely, THIOGLUCO-SIDE GLUCOHYDROLASE 4 (TGG4) and TGG5 and

PENETRATION 2 (PEN2) myrosinases are also strongly expressed in roots, among which PEN2 is known to be a crucial component of the plant innate immune system against microbial pathogens (Lipka *et al.*, 2005; Bednarek *et al.*, 2009), while the functional roles of TGG4 and TGG5 are yet to be addressed. Given the well-characterized roles of IG catabolites in interaction with microbes, it is plausible that these root-secreted compounds derived from glucosinolates and/or Trp play a role in root–microbe interactions. This idea is supported by a previous study showing that metabolic engineering of a foreign glucosinolate in *A. thaliana* impacted the assembly of the root-associated microbial community (root microbiota; Bressan *et al.*, 2009).

Here, we hypothesized that PYK10 mediates the hydrolysis of IGs and other Trp-derived specialized metabolites and the secretion of their terminal products into the rhizosphere, ultimately affecting the composition of root microbiota. By profiling the root microbiota shaped in the roots of mutants impaired in ER bodies and Trp-derived metabolic pathways grown in natural soil, we provide genetic evidence that these pathways are involved in the root microbiota assembly. We also show that this effect on microbial communities is partially mediated by root-exuded compounds and that lack of these pathways has a direct impact on (1) bacterial community composition in the absence of fungi and (2) fungal behavior in the absence of bacteria. Overall, our results demonstrate a physiological role for root ER bodies in modulating root microbiota assembly at the root–soil interface.

## Materials and Methods

### Plant, microbial, and soil materials

Three batches of Cologne agricultural soil (CAS) were harvested in February 2017 (CAS11), February 2019 (CAS13), and January 2020 (CAS15), respectively, as described previously (Bulgarelli *et al.*, 2012). *Arabidopsis thaliana* (L.) Heynh. wild-type (WT) Col-0 seeds were obtained from the Nottingham Arabidopsis Stock Centre (NASC). The *pyk10-1 bglu21-1* double mutant (*pyk10bglu21*), *nai1-1*, *myb34 myb51 myb122* triple mutant (*myb34/51/122*) and *cyp79b2 cyp79b3* double mutant (*cyp79b2b3*) plants have been described previously (Zhao *et al.*, 2002; Matsushima *et al.*, 2003b; Nagano *et al.*, 2009; Frerigmann & Gigolashvili, 2014). The bacterial and fungal strains used in this study (Supporting Information Tables S1, S2) were described previously (Bai *et al.*, 2015; Hiruma *et al.*, 2016; Mesny *et al.*, 2021).

### Root harvesting and fractionation

Plants were cultivated in pots containing CAS under long-day conditions in a glasshouse, where pots with different genotypes of plants were placed in a randomized design. Roots were then harvested and fractionated into the rhizosphere, rhizoplane, and endosphere fractions, as described previously (Duran *et al.*, 2018). Briefly, the soil particles loosely attached to the root ('rhizosphere') were collected by quickly shaking by hand in sterile water. Microbes on the root surface ('rhizoplane') were collected by vigorously shaking roots in a buffer containing a detergent by hand for 2 min, followed by filtration through a 0.22-μm membrane. Roots were then surface-sterilized with 70% (v/v) ethanol and bleach solution (sodium hypochlorite; *c.* 2% active chlorine) for 45–60 s each to obtain the 'endosphere' fraction. Soil from unplanted pots that underwent the same watering procedures next to plant-containing pots were collected as 'bulk soil' samples. All samples were immediately frozen in liquid nitrogen and stored at −80°C until processing.

### Collection of root exudates

Root exudates were collected from plants hydroponically grown in axenic glass jars containing glass beads, as described previously (Wippel *et al.*, 2021). Seeds of Col-0 WT, as well as *pyk10bglu21* and *cyp79b2b3* mutant plants, were surface-sterilized with 70% (v/v) ethanol and sodium hypochlorite with *c.* 2% (w/v) active chlorine and germinated on metal meshes placed on half-strength Murashige and Skoog (MS) media (Sigma-Aldrich) supplemented with 1% (w/v) sucrose and 1% (w/v) agar. Seeds were stratified for 48 h at 4°C in the dark and cultured for 4 d under short-day conditions (10 h under light at 21°C and 14 h under dark at 19°C). The 4-d-old seedlings on the mesh were transferred aseptically into glass jars containing sterile glass beads (1 mm) and 26 ml of half-strength liquid MS media. Glass jars were placed in a breathable Microbox (Sac O2, Belgium) and cultivated for 5 wk under short-day conditions. The hydroponic medium was collected using an aseptic stainless needle into 50-ml tubes and concentrated to *c.* 1/10 volume by a lyophilizer.

### Obtaining roots for metabolite profiling

To collect roots for metabolite analysis, Col-0 WT and *pyk10bglu21* and *cyp79b2b3* mutant plants were cultured on half-strength MS media supplemented with 1% (w/v) sucrose and 1% (w/v) agar for 5 wk under short-day conditions as described previously. Plates were placed into the D-Root system (Silva-Navas *et al.*, 2015). Roots were weighed, harvested, frozen in liquid nitrogen, and stored at −80°C until further processing. Frozen roots were homogenized in DMSO (Sigma-Aldrich) containing 0.5 mM camphorsulfonic acid and 0.5 mM lidocaine (Sigma-Aldrich) as internal standards, using 1-mm zirconia beads as described earlier (Wolinska *et al.*, 2021) and subjected to LC–MS analysis.

### Metabolite profiling of root extracts and root exudates

The LC–MS system consisted of the UltiMate 3000 RS (Thermo Fisher Scientific, Waltham, MA, USA) hyphenated to a TIMS-TOF mass spectrometer (Bruker Daltonics, Hamburg, Germany). Chromatographic separation was carried out on a ACQUITY UPLC HSS T3 C18 column (Waters, Milford, MA, USA; 2.1 × 150 mm, 1.8 μm particle size) at 22°C with a mobile phase flow rate of 0.25 ml min$^{-1}$. The elution was conducted using water containing 0.1% of formic acid (Sigma-Aldrich; Solvent A) and acetonitrile (VWR Chemicals, Fontenay-sous-Bois,

France) containing 0.01% of formic acid (Solvent B) in the following gradient: 0–5 min from 10% to 30% B, 5–12 min to 100% B, and 12–15 min maintained at 100% B. The mass spectrometer was operated using the following settings: ion source voltage of $-4.5$ or $4.5$ kV, nebulization of nitrogen at a pressure of 2.2 bar, and a gas flow rate of $10\,l\,min^{-1}$. Ion source temperature was 220°C. The spectra were scanned in positive and negative ionization in fragmentation mode (ddMSMS) at a range of 95–1000 $m/z$ at a resolution >30 000 FWHM (full width at half maximum). The spectrometer was calibrated with sodium formate salt clusters as internal calibrant before each analysis. The samples (5 µl) were injected into the inlet port after purging and rinsing the system. LC–MS system operation and data acquisition was supervised by Compass HyStar software (v.6.0; Bruker Daltonics). Obtained LC–MS data were processed for peak detection, deisotoping, alignment, and gap-filling by MS-DIAL v.4.74 (Tsugawa *et al.*, 2015) separately for positive and negative ionization modes, and then, data from both modes were combined. The prepared data table was postprocessed for missing values imputation, log transformation, and data filtering by MetaboAnalyst (Pang *et al.*, 2021). Then, data were visualized by sparse partial least squares discriminant analysis and Venn diagrams showing signals selected by one-way ANOVA with Benjamini–Hochberg correction with the following criteria: FDR $\leq 0.05$, and |log fold change| $\geq 1.0$, where fold change is calculated for specific comparison of *cyp79b2b3* vs Col-0 and *pyk10bglu21* vs Col-0. Glucosinolates and indole-3-acetamide were identified based on the MS/MS fragmentation spectra. Standard compounds were used for the identification of indole-3-acetonitrile, camalexin, indole-3-carboxylic acid, raphanusamic acid, esculetin, fraxetin, and scopoletin (Sigma-Aldrich). Heights of respective molecular ion peaks were used for quantification of identified metabolites. In case of root extracts, peak heights of signals of interest were additionally normalized to the peak height of the internal standard.

## Collection of root extracts

To collect root extracts, Col-0 WT and *pyk10bglu21* and *cyp79b2b3* mutant plants were cultured on half-strength MS media supplemented with 1% (w/v) sucrose and 1% (w/v) agar for 21 d under short-day conditions as described previously. Roots were weighed, harvested, frozen in liquid nitrogen, and stored at $-80$°C until further processing. Roots were homogenized in phosphobuffered saline using 1-mm zirconia beads to obtain $10\,mg\,ml^{-1}$ of root extracts immediately before treatment.

## Soil treatment with root exudates

Approximately 500 mg of CAS soil was transferred into 2-ml screw-cap tubes and treated with 50 µl of root exudates or root extracts. Tubes were covered by breathable tape and incubated at 28°C under dark conditions. Root exudates or freshly prepared root extracts were added every 3 d to replenish the weight loss due to the evaporation of the moisture content. Soils were freeze-dried and stored at $-80$°C until further processing.

## Bacterial microbiota reconstitution experiment

Bacterial cells were first grown on plates containing 50% trypsin soy broth (TSB; $15\,g\,l^{-1}$) supplemented with 1.5% (w/v) agar. Single colonies were then used to inoculate 50% TSB liquid media in 96-deep-well plates and cultured for 4 d at 25°C. Sixty microliters of cultures were transferred to another 96-well plate containing 600 µl of the sterile TSB media cultured for another 3 d in parallel to the original culture plates. Cultures from 7-d-old and 3-d-old plates were pooled, and optical absorbance at 595 nm was roughly normalized to each other using a plate reader (TECAN, Männedorf, Switzerland). Equal volumes of strains were then pooled into a new tube and centrifuged at 1800 $g$ for 10 min to remove the TSB, followed by two washes in 10 mM $MgCl_2$. The obtained pellet was dissolved in $MgCl_2$ at the $OD_{600}$ of 0.15–0.25, followed by overnight incubation at 25°C, such that bacteria would have consumed nutrients carried over from previous cultures and utilize the root exudate as their sole nutrient source during the treatment. On the day of treatment, the bacterial cells were collected by centrifuge and resuspended in 1/10 volume of 10 mM $MgCl_2$ and mixed with root exudates from respective genotypes to obtain $OD_{600}$ of 0.05, a part of which was further 1 : 10 diluted with the same root exudates to obtain $OD_{600}$ of 0.005. These bacterial SynCom samples were distributed to sterile 96-well microbial culture plates (50 µl per well) and incubated at 25°C without agitation. At the time of harvest (24 or 72 h postinoculation; 24 or 72 hpi), a fixed amount of *Escherichia coli* DH5α cells (at final $OD_{600}$ of 0.01 or 0.001 depending on the initial inoculum titer), whose 16S *rRNA* is fully distinguishable from all strains included in our SynCom, was added to each sample to enable quantitative abundance (QA) estimation (Lundberg *et al.*, 2021). The cultures were processed for DNA isolation immediately after adding the *E. coli* cells.

## DNA extraction and amplicon sequencing

Total DNA from the rhizosphere, rhizoplane, and root samples was extracted from collected soil, filter paper, and surface-sterilized root samples, respectively, using the FastDNA SPIN Kit for Soil (MP Biomedicals, Solon, OH, USA), as described previously (Duran *et al.*, 2018). For DNA extraction from bacterial SynCom, cells were lysed in alkaline sodium hydroxide and directly used as a PCR template, as described previously (Bai *et al.*, 2015). The V5–V7 region of the bacterial 16S rRNA gene and the ITS1 region of fungal DNA were PCR-amplified by specific primer sets containing adapter sequences for sequencing and barcode sequences for multiplexing (Tables S3–S6). Approximately the same amounts of PCR product were pooled, purified twice using AMPure XP beads (Beckman Coulter Agencourt, Brea, CA, USA), and sequenced by an Illumina MiSeq platform (MiSeq Reagent Kit V3, 600-cycle).

## Bioinformatic analysis of microbiome profiling

Preprocessing, demultiplexing, and analysis of amplicon sequence variants (ASVs) were performed as described previously (Harbort

*et al.*, 2020) using the DADA2 pipeline (Callahan *et al.*, 2019). Taxonomic assignments for ASVs were performed referring to the SILVA (v138) database for bacteria and UNITE (release 04.02.2020; Nilsson *et al.*, 2019) database for fungi. Reference-based analysis of bacterial SynCom data was performed using the Rbec pipeline (Zhang *et al.*, 2021).

### Statistical analysis for microbiome profiling

All statistical analyses were performed in R (https://www.r-project.org/). Unconstrained and constrained principal coordinates analyses (PCoA and CPCoA) were performed based on Bray–Curtis dissimilarities using the cmdscale and capscale functions in the STATS and VEGAN packages. Differential abundance of ASVs and aggregated ASVs was conducted using the EDGER package by fitting relative abundance to a generalized linear model with a negative binomial distribution, controlling for sequencing batch, technical replicates, and the experimental batch as random factors. The quantitative abundance of bacteria in SynCom was calculated by dividing the read counts per strain or for the overall community by the read counts of *E. coli*.

### Plant–fungi binary interaction assay

Fungal inoculation was performed as described previously (Frerigmann *et al.*, 2021; Mesny *et al.*, 2021). Approximately 50 mg of fungal mycelium was collected and homogenized in 10 mM MgCl$_2$, which was then used to inoculate surface-sterilized seeds. Plants and fungi were co-cultured on half-strength MS media supplemented with 1% (w/v) agar for 21 d under short-day conditions, and their shoot fresh weights were measured after cultivation.

## Results

### ER bodies and Trp-derived specialized metabolites together contribute to root microbiota assembly

To investigate the impact of ER bodies and Trp-derived specialized metabolites on root microbiota assembly, we prepared natural soils (Bulgarelli *et al.*, 2012) and grew *A. thaliana* mutants impaired in ER body-resident myrosinases (*pyk10bglu21*), the formation of ER bodies (*nai1-1*), the biosynthesis of IGs as well as other Trp-derived specialized metabolites to a milder extent (*myb34/51/122*), and the entire specialized Trp metabolism (*cyp79b2b3*), along with the Col-0 WT plants (Fig. 1b), and performed amplicon sequencing analysis of bacterial (16S *rRNA*) and fungal (ITS1) microbiota community compositions of roots (rhizoplane and endosphere fractions) as well as rhizosphere and bulk soil fractions. A constrained principal coordinates analysis (cPCoA) based on Bray–Curtis dissimilarities between samples at the amplicon sequence variant (ASV) level (Fig. 1c) revealed significant differences between the plant genotypes in the bacterial communities in the rhizoplane ($P = 0.009$; 5.40% of variation explained by genotypes) and in the fungal communities in the endosphere ($P = 0.021$; 11.41%; Table S7). On the contrary,

bacterial and fungal communities in the endosphere and rhizoplane, respectively, did not significantly differ across genotypes. Bacterial communities in the rhizoplanes of *cyp79b2b3* and *myb34/51/122* and of *pyk10bglu21* and *nai1* were similar to each other, respectively (Fig. 1c; top left), pointing to an active role of IGs and ER bodies in bacterial community assembly rather than a stochastic variation between different host genotypes. In fungal communities, only *cyp79b2b3* and *pyk10bglu21* mutants, in which enzyme-encoding genes were disrupted, showed substantial differences from the WT, while *myb34/51/122* and *nai1*, the transcription factor mutants, exhibited a milder impact (Fig. 1c; bottom right). This may be explained by Trp-derived metabolites other than IGs accumulating to levels similar to Col-0 and/or residual amounts of IGs and PYK10 and BGLU21 in these mutant roots (Matsushima *et al.*, 2004; Frerigmann *et al.*, 2016). A similar trend of microbial community shifts in mutants compared with the WT was observed when we aggregated the relative abundance (RA) of ASVs at the family level (Fig. S1). We also observed that the root-associated microbial communities were not dominated by a small subset of ASVs (Fig. S2). These analyses showed that the observed community shift occurred at the family or higher taxonomic level rather than at the strain- or species-specific level.

We noted that the bacterial community shift observed in the rhizoplane of mutants compared with the WT was in the same direction along the first axis, while the ER body mutants and Trp metabolism mutants were separated along the second axis (Fig. 1c; top left). This implied that the loss of ER bodies and Trp-derived metabolites exerted a partly similar impact, if not entirely identical, on the root-associated microbiota structure. This was also supported by the significant positive correlation between the log$_2$-scale fold changes (logFC) in RA values of ASVs or families between each mutant and the WT (Figs S3–S5). Overall, these data demonstrate that the ER body-resident myrosinases and Trp metabolism contribute to root microbial community assembly, affecting the behavior of distinct but overlapping sets of microbes.

### ER body-resident myrosinases contribute to the secretion of Trp specialized metabolites, potentially produced from IGs

The significant bacterial community shift at the rhizoplane (root exterior) suggested a role for root-exuded compounds in bacterial community assembly. However, it remained unknown whether and how PYK10 and BGLU21 intracellularly stored in ER bodies could contribute to the extracellular secretion of metabolites into the rhizosphere. We aimed to test this directly by collecting root exudates from Col-0 WT and *pyk10bglu21* and *cyp79b2b3* mutant plants, axenically grown in a hydroponic culture system (Wippel *et al.*, 2021) and analyzing it by untargeted HPLC-MS/MS. This revealed a significant difference in the compositions of metabolites between exudates collected from mutants and the WT (Fig. 2a), indicating that ER body-resident PYK10 and BGLU21 are involved in the cellular metabolism, intracellularly and/or extracellularly, and influence the profile of metabolites ultimately secreted to the rhizosphere. We observed up to 696
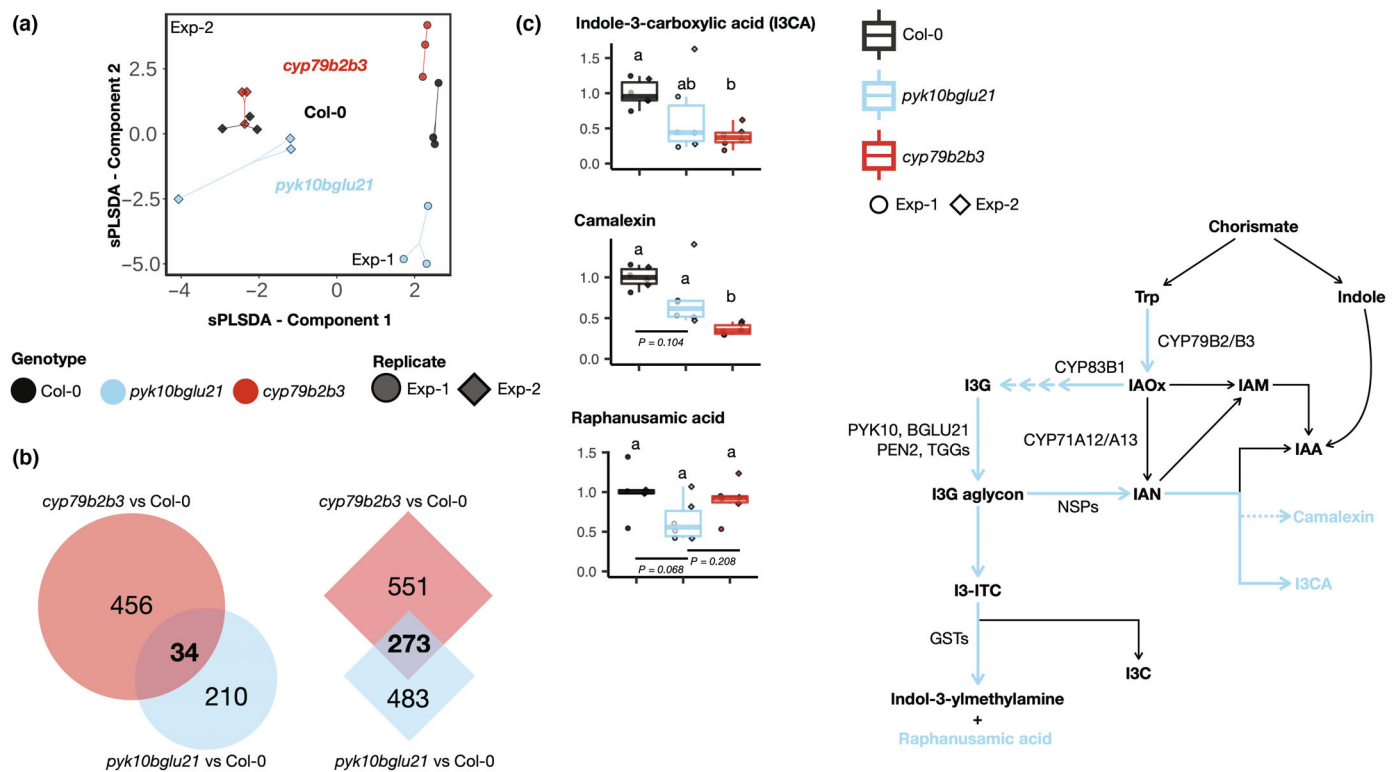
**Fig. 2** Root secretion of Trp-derived metabolites is partly dependent on PYK10 and BGLU21. (a) Sparse partial least squares discriminant analysis plot of profiles of signals corresponding to root-exuded metabolites. Colors and shapes represent the genotypes and biological replicates, respectively. (b) Venn diagrams representing the differentially abundant MS signals detected in *cyp79b2b3* and *pyk10bglu21* mutant media compared with Col-0 for each biological replicate (moderated *t*-test; false discovery rate $\leq 0.05$ and $|\log_2$ fold change$| \geq 1.0$). (c) The abundance of indole-3-carboxylic acid (I3CA), camalexin, and raphanusamic acid, normalized to respective Col-0 samples, are shown as box plots. A schematic overview of the Trp metabolic pathway is also shown. Blue letters indicate the metabolites whose abundances are shown in the boxplots, and blue arrows indicate possible paths through which these metabolites can be affected by PYK10 and BGLU21. Letters indicate statistical significance corresponding to the analysis of variance (ANOVA) and *post hoc* Tukey's honestly significant difference (HSD) tests ($\alpha = 0.05$). Marginal *P* values are shown with numbers. Median, interquartile range (IQR), and data points within $\pm 1.5 \ast$IQR are indicated by horizontal lines, boxes, and whiskers, respectively, along with the raw data points whose shapes correspond to individual experiments.

and 1307 signals with significant differences in their RA values in *pyk10bglu21* and/or *cyp79b2b3* root exudates compared with Col-0 exudates, among which 34 and 273 signals were commonly depleted/enriched in both mutant exudates (Fig. 2b). The overall difference in the metabolomic profiles was larger in *pyk10bglu21* than in *cyp79b2b3* (Fig. 2a), consistent with the broad range of substrates for ER-resident myrosinases, including but not limited to Trp-derived specialized metabolites (Matsushima *et al.*, 2003b; Ahn *et al.*, 2010; Nakano *et al.*, 2017; Nakazaki *et al.*, 2019; Yamada *et al.*, 2020).

We then identified a wide range of glucosinolates and Trp specialized metabolites, along with coumarins, in our dataset based on standards or MS/MS fragmentation spectra (Figs 2c, S6a–d; Table S8). Among the tested compounds, we revealed that indole-3-carboxylic acid (I3CA) and camalexin were significantly different between genotypes. We also noted that the abundance of raphanusamic acid tends to be lower in *pyk10bglu21* exudates compared with Col-0 exudates, albeit not statistically significant after correction for multiple comparisons ($P = 0.068$). On the contrary, we did not observe a significant difference in the abundance of IGs, indole-3-acetamide (IAM), and indole-3-

acetonitrile (IAN). We noted that the abundance normalized to the total ion chromatogram of these metabolites is low and that even *cyp79b2b3* exudates did not show any difference compared with Col-0 exudates, while these compounds were highly abundant in root extracts harvested from plants grown without light exposure (Fig. S6e). It was therefore inferred that these compounds are not substantially secreted to the rhizosphere in our experimental setup, and the peaks we observed were within the range of detection background. Notably, I3CA and camalexin are both exclusively produced from IAN, while IAN can be produced as a catabolic product of I3G hydrolysis by myrosinases as well as directly from indole-3-acetaldoxime (IAOx). Nitrile formation from IG aglycones is facilitated by a group of proteins called NITRILE SPECIFIER PROTEINS (NSPs), many of which are strongly co-expressed with PYK10 and other ER body-related genes (Nakano *et al.*, 2017). This, together with our results, suggests that PYK10-mediated I3G catabolism produces IAN, which is then fed into the biosynthetic pathways of I3CA and camalexin, although *in planta* camalexin production from I3G-derived IAN has not been characterized to date. Overall, this result demonstrates that Trp-derived specialized metabolites are
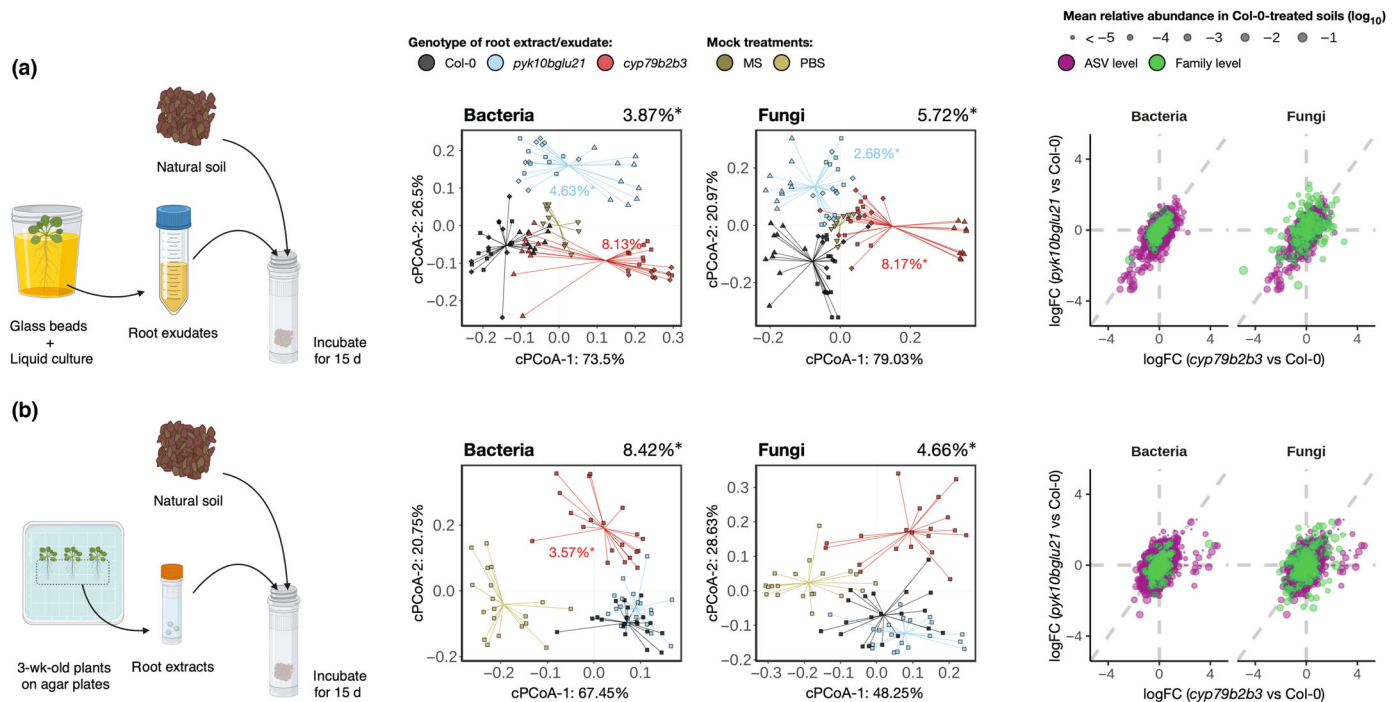
**Fig. 3** Compounds secreted into the rhizosphere in a PYK10- and BGLU21-dependent manner have an impact on microbial community assembly in the soil environment. Soils were treated with root exudates (a) or root extracts (b) consecutively for 15 d with 2-d intervals. Constrained principal coordinates analysis (cPCoA) plots are based on Bray–Curtis dissimilarities of bacterial (left) and fungal (right) communities, and the ordination was constrained by genotypes and conditioned by biological and technical replicates. The scatter plots show a comparison of changes in the relative abundance of amplicon sequence variants (ASVs; magenta) or families (green) in soils treated with mutant root exudates/extracts compared with soils treated with Col-0 root exudates/extracts. Size corresponds to their mean relative abundance in soils treated with Col-0 root exudates/extracts. Variation explained by genotypes based on permutational analysis of variance (PERMANOVA; *n* = 1000) is indicated at top right, and asterisks indicate its statistical significance (α = 0.05).

indeed secreted to the rhizosphere and implies the possibility that PYK10 and BGLU21 either directly or indirectly contribute to the secretion of these metabolites as well as other metabolites.

### Trp-derived metabolites secreted into the rhizosphere in a manner dependent on PYK10 and BGLU21 are capable of modulating microbiota community structure

We then tested whether the observed difference in root exudation profiles would affect microbial community assembly processes by treating natural soils with these different root exudates and analyzing the resulting bacterial and fungal community structures (Fig. 3a; Table S9). Given the major variation between experimental batches (Fig. S6f,g), while the overall trend was similar, we decided to focus on one batch of exudate samples for further experiments (note that each batch contained three technical replicates, where plants were grown independently in different pots). We found that, after 15 d of consecutive treatments with 2-d intervals, the soil microbial communities exhibited a shift compared with those from mock-treated soils, which is consistent with a previous study (Badri *et al.*, 2013), in a manner dependent on the genotypes of origin of the root exudates (Fig. 3a; middle panels). Both bacterial and fungal communities in the soils treated with *pyk10bglu21* or *cyp79b2b3* exudates were significantly different from each other and from the communities in the soils treated with Col-0 exudates. The logFC in their RA values relative to the WT controls was positively correlated between

*pyk10bglu21* and Col-0 and *cyp79b2b3* and Col-0, at both the ASV and the family levels (Fig. 3a; right panel), suggesting the presence of a group of microbes that are targeted by the metabolites whose secretion to the rhizosphere is dependent of Trp specialized metabolism and ER body-resident myrosinases.

Next, to test whether PYK10 and BLGLU21 also contribute to the biosynthesis or accumulation in roots or only to the secretion of the bioactive metabolites responsible for the observed community shifts or also their accumulation in roots, we prepared axenic root crude extracts (homogenates) from these genotypes and performed the same soil treatment experiment (Fig. 3b; Table S9). The root extract treatments also triggered significant community shifts in the soil microbial community compared with mock-treated soils (Fig. 3b; middle panels). Interestingly, the cPCoA plots showed that Col-0 and *pyk10bglu21* root extracts triggered similar shifts in the microbial community compositions, while treatments with *cyp79b2b3* root extracts resulted in significantly different community structures. Comparison of logFC in RA values of ASVs and families also pointed to the presence of a group of microbes that were specifically affected by the CYP79B2 and CYP79B3 pathway but not by the PYK10 and BGLU21 pathway (Fig. 3b, right panel). These findings suggest that the Trp specialized metabolites in Col-0 root extracts that were responsible for the observed community assembly are not secreted from *pyk10bglu21* roots but they (or their glycosylated precursors) accumulate in roots. *A. thaliana* roots accumulate many myrosinases that are not stored in ER bodies, such as TGG4, TGG5, and PEN2 (Millet *et al.*, 2010; Fu
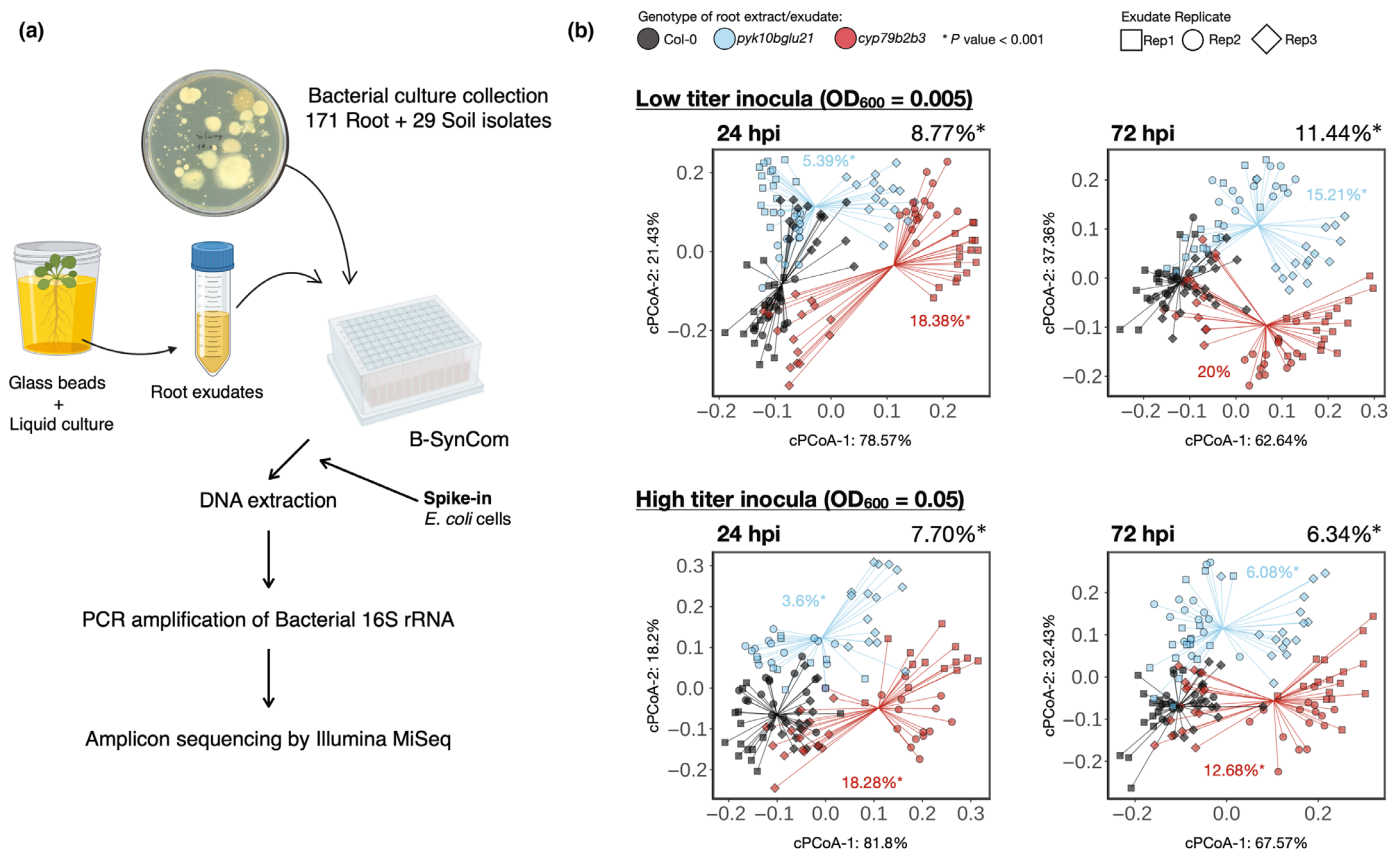
**Fig. 4** Compounds secreted into the rhizosphere in a PYK10- and BGLU21-dependent manner have a direct impact on bacterial community assembly. (a) Schematic representation of experiments using a bacterial SynCom composed of 171 root-derived and 29 soil-derived isolates. (b) Constrained principal coordinates analysis (cPCoA) analysis of bacterial communities in root exudates from Col-0 (black), *pyk10bglu21* (blue) and *cyp79b2b3* (red) at 24 and 72 h postinoculation (hpi) using Bray–Curtis dissimilarities based on the relative abundance. Shapes correspond to the individual replicates of root exudates. Ordination was constrained by genotypes and conditioned by biological and technical replicates. Variance explained by genotypes based on the permutational analysis of variance (PERMANOVA; $n = 1000$) is indicated at top right, and asterisks indicate its statistical significance ($\alpha = 0.05$).

*et al.*, 2016), which are capable of catalyzing the same reaction as PYK10 and BGLU21 when subcellular membrane partitions are artificially disrupted in a homogenate. Therefore, the active compounds may be accumulated in *pyk10bglu21* roots either in an already active form or in an inactive glycosylated form. Overall, these results suggest a role for Trp-derived metabolites whose secretion but not accumulation depends on ER body myrosinases in modulating microbial community structures. It needs to be noted that, besides the microbes that are commonly affected in *pyk10bglu21* and *cyp79b2b3* roots, root exudates, and root extracts, these mutants also triggered a community shift unique to each genotype (note the separation of these genotypes in CPCoA plots). This, along with the metabolomic profiling data of root exudates, points to the presence of PYK10 and BGLU21 substrates that are derived from other precursors than Trp, which are also capable of manipulating microbial community compositions.

## Root-exuded compounds directly affect bacterial community structure independently of fungi

Trp-derived metabolites, including IGs, have been reported to be crucial for interaction with endophytic fungi (Hiruma *et al.*, 2016; Wolinska *et al.*, 2021), while their impact on bacteria is

less understood. To assess the direct impact of root exudates on bacterial community assembly, we performed a synthetic community (SynCom) profiling experiment in these root exudates (Fig. 4a), using 171 bacterial strains isolated from healthy *A. thaliana* roots grown in natural soil and 29 strains isolated from the same, unplanted soil (Bai *et al.*, 2015). The analysis of β-diversity based on RA values revealed that the SynCom compositions in the Col-0 root exudates were significantly different from the composition in the mutant root exudates (Fig. 4b; Table S10). The effect on bacterial community composition was more different between Col-0 and *cyp79b2b3* exudates than between Col-0 and *pyk10bglu21* exudates, which is similar to what was observed in the soil treatment experiment (Fig. 3). The community shift in mutants compared with Col-0 was significant with both initial titers ($OD_{600}$ of 0.05 and 0.005) and at both time points (24 and 72 hpi). The overall variance explained by genotypes was larger when we used a lower titer as a starting inoculum, and we observed a higher level of overall community growth (increase in the total number of bacterial cells within the community measured by the quantitative abundance normalized to *E. coli* cells spiked in before DNA extraction) under the low-titer than high-titer conditions, while between genotypes, the overall community growth was largely similar (Fig. S7a). When

we compared the community structure dynamics over time within genotypes, we observed a more dynamic community assembly at 24 hpi when we used low-titer inoculum, with eventual convergence on a similar community structure at 72 hpi (Fig. S7b). These data suggest that the contribution of ER bodies and Trp-derived specialized metabolites to community assembly is larger when bacterial cells are metabolically more active and undergoing dynamic community re-assembly. We compared the growth of each bacterial strain in Col-0 and mutant exudates (Fig. S7c) and found a small group of strains that showed a similar response in mutant exudates in comparison with Col-0 exudates (Fig. S7d), pointing to a set of bacteria commonly targeted by these pathways via root-exuded compounds. Overall, these results suggest that Trp-derived metabolites secreted to the rhizosphere in a PYK10 and BGLU21-dependent manner can directly impact the bacterial community assembly in the absence of eukaryotic organisms, such as plants and fungi.

## ER bodies and Trp-derived metabolites directly influence plant–fungus interactions

Lastly, we tested whether the ER body pathway and the Trp metabolic pathway have a direct impact also on the plant–fungus interaction in the absence of bacteria. Toward this end, we inoculated the same set of plants (Col-0, *pyk10bglu21*, and *cyp79b2b3*) in a mono-association setup (Frerigmann *et al.*, 2021; Fig. 5) with fungal strains isolated from roots or leaves of healthy *A. thaliana* and related species grown in natural soils (Hiruma *et al.*, 2016; Mesny *et al.*, 2021). We found that the growth of *cyp79b2b3* mutant plants was severely impaired by more than half of the strains compared with the WT plants (24 isolates), especially by those belonging to the classes Leotiomycetes and Dothideomycetes. Furthermore, seven strains were found to significantly impair the growth of both *cyp79b2b3* and *pyk10bglu21* mutants compared with Col-0. On the contrary, 16 isolates, including all those belonging to the class Leotiomycetes, specifically restricted the growth of *cyp79b2b3* but not *pyk10bglu21* plants, and three strains showed a negative impact only on *pyk10bglu21* compared with the Col-0 WT. These results demonstrate that the myrosinases stored in ER bodies and Trp-derived metabolites directly regulate plant–fungus interactions and target distinct but overlapping sets of fungal strains. Combined with the results that the ER body and Trp-derived metabolic pathways together contribute to the bacterial and fungal community assembly at the rhizoplane and in the endosphere, respectively, our overall findings illustrate a role for ER body-resident myrosinase-mediated Trp metabolism in root–microbiota interactions.

## Discussion

### The physiological role of root ER bodies in root–microbiota interactions via root-secreted metabolites

ER bodies in *A. thaliana* are abundant both in leaves (inducible ER bodies) and roots (constitutive ER bodies). While the role of leaf ER bodies in interaction with herbivorous animals and

pathogenic bacteria has been characterized, the role of root ER bodies remained unclear. Here, we provide clear evidence that root ER bodies and the myrosinases therein are involved in root–microbiota interactions, whose processes are at least partially mediated by root-secreted Trp specialized metabolites. In the early era of ER body/dilated cisternae research, a functional link between ER bodies and glucosinolates was already proposed, given their co-occurrence in a group of families within the order Brassicales (Iversen, 1970), which was further supported by the recent discovery of myrosinase activity in PYK10 and BGLU18 (Nakano *et al.*, 2014, 2017; Nakazaki *et al.*, 2019). This also explains the role of leaf ER bodies in antiherbivorous defense (Nakazaki *et al.*, 2019; Yamada *et al.*, 2020). Overall, our findings are in line with previous predictions that the physiological functions of ER bodies are associated with glucosinolates. Furthermore, we clearly demonstrated that ER body-resident myrosinases are involved in the secretion of metabolites into the rhizosphere, whose underlying mechanisms remain to be addressed. A plausible scenario is that the deglycosylation of intracellularly accumulated metabolites by PYK10 and BGLU21 stimulates the secretion of their aglycons to the apoplast. This possibility has been reported for scopolin, whose deglycosylation by a cytosolic enzyme BGLU42 is necessary for the rhizospheric secretion of its aglycon, scopoletin (Stringlis *et al.*, 2018). Alternatively, it also remains possible that a part of PYK10 and BGLU21 proteins are secreted to the apoplast or deposited to the rhizoplane through the secretory pathway from the ER, thereby metabolizing the glucosides secreted from root tissues.

### Potential *in planta* substrates of PYK10 and BGLU21 responsible for the microbiota assembly

Trp-derived specialized metabolites are widely crucial for interactions with microbes (Pedras *et al.*, 2011; Pastorczyk & Bednarek, 2016), including root microbiota (Wolinska *et al.*, 2021), and our findings suggest that a part of the physiological substrates of ER body-resident myrosinases are derived from Trp. Partially similar community shift observed in *myb34/51/122* and *pyk10bglu21* suggests IGs as potential *in planta* substrates of PYK10 and BGLU21, which is consistent with the transcriptional co-regulation of these pathways (Nakano *et al.*, 2017). On the contrary, we did not detect a striking difference in the abundance of intact glucosinolates or its well-characterized terminal product IAN in the root-secreted metabolome. In contrast, we observed a reduction in the relative abundance of other Trp-derived metabolites, including camalexin and I3CA. Both metabolites can be produced from IAN, which is one of the terminal products of I3G catabolism, implying the possibility that PYK10-mediated I3G hydrolysis feeds the precursor for Trp metabolism apart from IG biosynthesis (Fig. 2). On the contrary, *PYK10* and other ER body-related genes are strongly co-expressed with *CYP81F4* (Nakano *et al.*, 2017), encoding an enzyme to produce 1-methoxy I3G (1MI3G) from I3G, and 1MI3G is the most abundant form of IGs in the roots of Col-0 plants (Brown *et al.*, 2003). As methoxylated IAN cannot be a precursor for I3CA, and camalexin, it is inferred that there are other catabolic
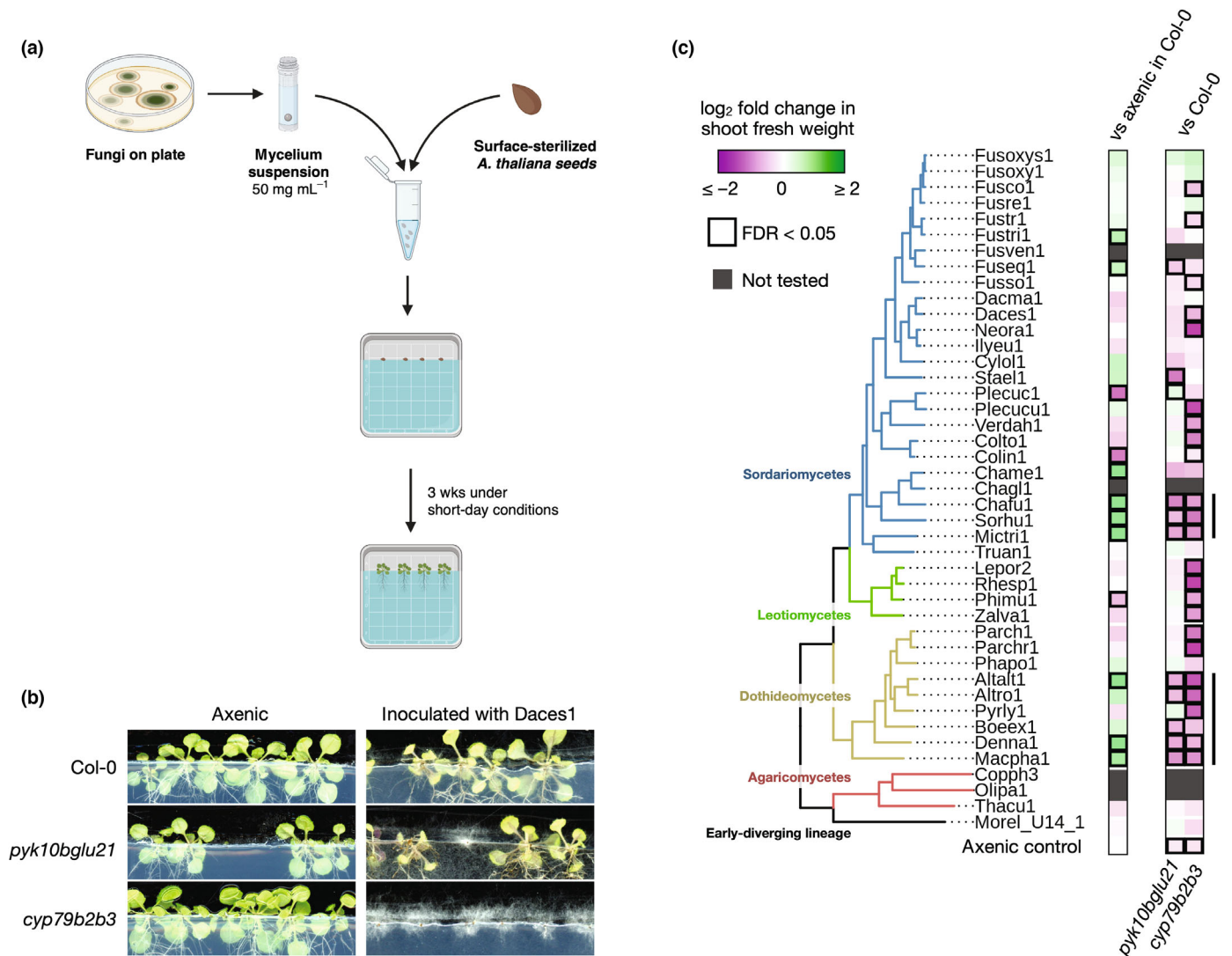
**Fig. 5** ER bodies and Trp metabolism are needed for an appropriate accommodation of endophytic fungi. (a) Schematic representation of experimental setup using a set of endophytic fungi isolated from healthy plant roots. (b) Representative images of plants inoculated with fungi along with axenic control plants. (c) A phylogenetic tree of fungi used in this study along with their impact on Col-0 growth compared with the axenic plants (left panel) and the impact of *pyk10bglu21* and *cyp79b2b3* mutations on shoot growth with respect to Col-0 plants inoculated with the same fungal strain. Marked with bold lines are false discovery rate ≤ 0.05 and |log₂ fold changes| ≥ 0.5.

products than those potentially fed into I3CA/camalexin pathways, which may also be responsible for the root-associated microbiota assembly. Importantly, however, it needs to be noted that the compounds we identified by standards or MS/MS spectra are a small minor proportion of root exudate metabolome, and there are yet many other unidentified metabolites whose abundance appeared to be dependent on PYK10 and BGLU21, and/or CYP79B2 and CYP79B3, which might play a crucial role in root microbiota assembly. Moreover, albeit a partial similarity, mutants impaired in Trp metabolism and mutants impaired in ER body system accommodate substantially distinctive microbial communities in their roots, demonstrating a role of pathway-specific impact on microbiota assembly, which can be explained by the fact that PYK10 is also capable of hydrolyzing

nonglucosinolate glucosides (Ahn *et al.*, 2010). A future study is needed to specify the identity of metabolites responsible for the observed community shift and to reveal its metabolic pathway(s).

Camalexin operates as an antimicrobial compound and affects microbial behavior directly (Bednarek *et al.*, 2005), while I3CA has been shown to mediate β-aminobutyric acid-triggered priming of immune responses and to covalently bind to cell wall oligosaccharides upon infection in *A. thaliana* (Hagemeier *et al.*, 2001; Tan *et al.*, 2004; Gamir *et al.*, 2012, 2018). The role of root-produced camalexin in regulating root-commensal interaction has also been reported (Koprivova *et al.*, 2019, 2023), which is in line with the role of specialized metabolites in interaction with microbes in a wide range of plant species (Singh *et al.*, 2022). Interestingly, camalexin exudation appears to play a

positive role in accommodating a plant growth-promoting bacterial commensal CH267 (Koprivova *et al.*, 2019, 2023), illustrating its function not only as an antimicrobial but also for recruiting beneficial microbes. Therefore, it is possible that camalexin and I3CA produced from IAN via IG metabolism directly influence root microbiota assembly. On the contrary, however, it needs to be noted that camalexin and I3CA are among the variety of metabolites whose relative abundance in root exudates is altered in *pyk10bglu21* and *cyp79b2b3* mutants (Fig. 2a), and the characteristics of other Trp metabolites whose secretion depends on ER body-resident myrosinases are yet to be identified. Further studies are needed to address which of these catabolic products are crucial for the interaction with root microbiota and to disentangle whether PYK10 and BGLU21 only contribute to the secretion of these metabolites or also to their biosynthesis.

It is also important to consider the fact that the exudates used in our experiments were collected from axenic, naïve plants, that is, in the absence of microbes or any immune elicitors. It has been well described that plant immune status has an impact on root metabolomic profiles (Millet *et al.*, 2010; Koprivova *et al.*, 2019) as well as on root exudation profiles (Bednarek *et al.*, 2005; Badri & Vivanco, 2009; Koprivova *et al.*, 2020, 2023). Therefore, it is likely that the metabolomic profile of root exudates may be substantially different between axenic and soil conditions. It also needs to be noted that the root exudation profiles were significantly distinct between the two biological replicates performed in this study. In order to avoid overly stochastic microbial behavior triggered by the metabolic fluctuation, we decided to focus on one biological replicate and rather repeated the soil and SynCom treatments multiple independent times to support reproducibility. Our approach has provided meaningful insight into how microbial community assembly is affected by metabolites that were differentially abundant in these exudate samples, while an independent experiment using independent exudate samples might trigger quantitatively different microbial responses. Moreover, root exudation is one of many aspects of root physiology, and our soil treatment experiments may not necessarily recapitulate the entire interaction occurring at the root–soil interface. Nonetheless, given that the three independent approaches employed in this study all suggested an overlapping role of Trp-derived metabolites and ER body-resident myrosinases, we propose a model according to which Trp-derived metabolites that are secreted in a manner dependent on PYK10 and BGLU21 under axenic naïve conditions are capable of manipulating a microbial community. Further studies will address to which extent our insights into the activity of axenic root exudates can be generalized to explain the actual microbial community shift observed in the glasshouse experiment.

## Acknowledgements

## Competing interests

None declared.

## Author contributions

RTN conceived and designed the project. AKB and RTN performed the glasshouse experiments. AKB collected root exudates and performed the soil treatment and bacterial SynCom experiments. AP and PB performed the metabolomic profiling of root exudates, and AP analyzed the data. AKB, JH and GMT performed the fungal inoculation experiment. RG, PZ and RG-O processed amplicon sequencing data, and AKB and RTN analyzed the obtained data. FG and SH designed and established the primers for amplicon sequencing, and SH established the fungal culture collection. AKB, KS, PB, KY and RTN interpreted the results. AKB, PB, KY and RTN wrote the manuscript.

## ORCID

Arpan Kumar Basak (iD) https://orcid.org/0000-0002-5005-1848
Paweł Bednarek (iD) https://orcid.org/0000-0002-3064-7775
Ruben Garrido-Oter (iD) https://orcid.org/0000-0003-1769-892X
Rui Guan (iD) https://orcid.org/0000-0003-0862-2368
Stephane Hacquard (iD) https://orcid.org/0000-0003-2293-3525
Ryohei Thomas Nakano (iD) https://orcid.org/0000-0001-5973-2300
Anna Piasecka (iD) https://orcid.org/0000-0002-0983-7507
Kazimierz Strzałka (iD) https://orcid.org/0000-0002-8367-4865
Gözde Merve Türksoy (iD) https://orcid.org/0000-0002-9472-205X
Kenji Yamada (iD) https://orcid.org/0000-0003-4872-3729
Pengfan Zhang (iD) https://orcid.org/0000-0002-7504-8397

## Data availability

The raw sequences are available at the European Nucleotide Archive (ENA) under accession no. PRJEB54088. The scripts used for processing the Illumina reads and statistical analyses are

available at https://github.com/Guan06/DADA2_pipeline and https://github.com/arpankbasak/ERBody_RootMicrobiota.

## References

**Ahn YO, Shimizu B-i, Sakata K, Gantulga D, Zhou Z, Bevan DR, Esen A. 2010.** Scopolin-hydrolyzing β-glucosidases in roots of *Arabidopsis*. *Plant and Cell Physiology* **51**: 132–143.

**Badri DV, Chaparro JM, Zhang RF, Shen QR, Vivanco JM. 2013.** Application of natural blends of phytochemicals derived from the root exudates of Arabidopsis to the soil reveal that phenolic-related compounds predominantly modulate the soil microbiome. *Journal of Biological Chemistry* **288**: 4502–4512.

**Badri DV, Vivanco JM. 2009.** Regulation and function of root exudates. *Plant, Cell & Environment* **32**: 666–681.

**Bai Y, Muller DB, Srinivas G, Garrido-Oter R, Potthoff E, Rott M, Dombrowski N, Munch PC, Spaepen S, Remus-Emsermann M *et al*. 2015.** Functional overlap of the Arabidopsis leaf and root microbiota. *Nature* **528**: 364–369.

**Bednarek P, Pislewska-Bednarek M, Svatos A, Schneider B, Doubsky J, Mansurova M, Humphry M, Consonni C, Panstruga R, Sanchez-Vallet A *et al*. 2009.** A glucosinolate metabolism pathway in living plant cells mediates broad-spectrum antifungal defense. *Science* **323**: 101–106.

**Bednarek P, Schneider B, Svatos A, Oldham NJ, Hahlbrock K. 2005.** Structural complexity, differential response to infection, and tissue specificity of indolic and phenylpropanoid secondary metabolism in *Arabidopsis* roots. *Plant Physiology* **138**: 1058–1070.

**Bonnett HT, Newcomb EH. 1965.** Polyribosomes and cisternal accumulations in root cells of radish. *Journal of Cell Biology* **27**: 423–432.

**Bressan M, Roncato MA, Bellvert F, Comte G, Haichar FE, Achouak W, Berge O. 2009.** Exogenous glucosinolate produced by *Arabidopsis thaliana* has an impact on microbes in the rhizosphere and plant roots. *ISME Journal* **3**: 1243–1257.

**Brown PD, Tokuhisa JG, Reichelt M, Gershenzon J. 2003.** Variation of glucosinolate accumulation among different organs and developmental stages of *Arabidopsis thaliana*. *Phytochemistry* **62**: 471–481.

**Bulgarelli D, Rott M, Schlaeppi K, van Themaat EVL, Ahmadinejad N, Assenza F, Rauf P, Huettel B, Reinhardt R, Schmelzer E *et al*. 2012.** Revealing structure and assembly cues for Arabidopsis root-inhabiting bacterial microbiota. *Nature* **488**: 91–95.

**Callahan BJ, Wong J, Heiner C, Oh S, Theriot CM, Gulati AS, McGill SK, Dougherty MK. 2019.** High-throughput amplicon sequencing of the full-length 16S rRNA gene with single-nucleotide resolution. *Nucleic Acids Research* **47**: e103.

**Clay NK, Adio AM, Denoux C, Jander G, Ausubel FM. 2009.** Glucosinolate metabolites required for an *Arabidopsis* innate immune response. *Science* **323**: 95–101.

**Duran P, Thiergart T, Garrido-Oter R, Agler M, Kemen E, Schulze-Lefert P, Hacquard S. 2018.** Microbial interkingdom interactions in roots promote Arabidopsis survival. *Cell* **175**: 973–983.

**Frerigmann H, Gigolashvili T. 2014.** MYB34, MYB51, and MYB122 distinctly regulate indolic glucosinolate biosynthesis in *Arabidopsis thaliana*. *Molecular Plant* **7**: 814–828.

**Frerigmann H, Piotrowski M, Lemke R, Bednarek P, Schulze-Lefert P. 2021.** A network of phosphate starvation and immune-related signaling and metabolic pathways controls the interaction between *Arabidopsis thaliana* and the beneficial fungus *Colletotrichum tofieldiae*. *Molecular Plant–Microbe Interactions* **34**: 560–570.

**Frerigmann H, Pislewska-Bednarek M, Sanchez-Vallet A, Molina A, Glawischnig E, Gigolashvili T, Bednarek P. 2016.** Regulation of pathogen-triggered tryptophan metabolism in *Arabidopsis thaliana* by MYB transcription factors and indole glucosinolate conversion products. *Molecular Plant* **9**: 682–695.

**Fu LL, Wang M, Han BY, Tan DG, Sun XP, Zhang JM. 2016.** Arabidopsis myrosinase genes AtTGG4 and AtTGG5 are root-tip specific and contribute to auxin biosynthesis and root-growth regulation. *International Journal of Molecular Sciences* **17**: 892.

**Gamir J, Pastor V, Cerezo M, Flors V. 2012.** Identification of indole-3-carboxylic acid as mediator of priming against *Plectosphaerella cucumerina*. *Plant Physiology and Biochemistry* **61**: 169–179.

**Gamir J, Pastor V, Sanchez-Bel P, Agut B, Mateu D, Garcia-Andrade J, Flors V. 2018.** Starch degradation, abscisic acid and vesicular trafficking are important elements in callose priming by indole-3-carboxylic acid in response to *Plectosphaerella cucumerina* infection. *The Plant Journal* **96**: 518–531.

**Hagemeier J, Schneider B, Oldham NJ, Hahlbrock K. 2001.** Accumulation of soluble and wall-bound indolic metabolites in *Arabidopsis thaliana* leaves infected with virulent or avirulent *Pseudomonas syringae* pathovar tomato strains. *Proceedings of the National Academy of Sciences, USA* **98**: 753–758.

**Hara-Nishimura I, Matsushima R. 2003.** A wound-inducible organelle derived from endoplasmic reticulum: a plant strategy against environmental stresses? *Current Opinion in Plant Biology* **6**: 583–588.

**Harbort CJ, Hashimoto M, Inoue H, Niu YL, Guan R, Rombola AD, Kopriva S, Voges MJEEE, Sattely ES, Garrido-Oter R *et al*. 2020.** Root-secreted coumarins and the microbiota interact to improve iron nutrition in Arabidopsis. *Cell Host & Microbe* **28**: 825–837.

**Hayashi Y, Yamada K, Shimada T, Matsushima R, Nishizawa N, Nishimura M, Hara-Nishimura I. 2001.** A proteinase-storing body that prepares for cell death or stresses in the epidermal cells of Arabidopsis. *Plant and Cell Physiology* **42**: 894–899.

**Hiruma K, Gerlach N, Sacristan S, Nakano RT, Hacquard S, Kracher B, Neumann U, Ramirez D, Bucher M, O'Connell RJ *et al*. 2016.** Root endophyte *Colletotrichum tofieldiae* confers plant fitness benefits that are phosphate status dependent. *Cell* **165**: 464–474.

**Hiruma K, Onozawa-Komori M, Takahashi F, Asakura M, Bednarek P, Okuno T, Schulze-Lefert P, Takano Y. 2010.** Entry mode-dependent function of an indole glucosinolate pathway in Arabidopsis for nonhost resistance against anthracnose pathogens. *Plant Cell* **22**: 2429–2443.

**Iversen T-H. 1970.** Cytochemical localization of myrosinase (β-thioglucosidase) in root tips of *Sinapis alba*. *Protoplasma* **71**: 451–466.

**Koprivova A, Schuck S, Jacoby RP, Klinkhammer I, Welter B, Leson L, Martyn A, Nauen J, Grabenhorst N, Mandelkow JF *et al*. 2019.** Root-specific camalexin biosynthesis controls the plant growth-promoting effects of multiple bacterial strains. *Proceedings of the National Academy of Sciences, USA* **116**: 15735–15744.

**Koprivova A, Schwier M, Volz V, Kopriva S. 2023.** Shoot-root interaction in control of camalexin exudation in Arabidopsis. *Journal of Experimental Botany* **74**: 2667–2679.

**Koprivova A, Volz V, Kopriva S. 2020.** Shoot-root interaction in control of camalexin exudation in Arabidopsis. *bioRxiv*. doi: 10.1101/2020.12.15. 422875.

**Lahrmann U, Strehmel N, Langen G, Frerigmann H, Leson L, Ding Y, Scheel D, Herklotz S, Hilbert M, Zuccaro A. 2015.** Mutualistic root endophytism is not associated with the reduction of saprotrophic traits and requires a noncompromised plant innate immunity. *New Phytologist* **207**: 841–857.

**Lipka V, Dittgen J, Bednarek P, Bhat R, Wiermer M, Stein M, Landtag J, Brandt W, Rosahl S, Scheel D *et al*. 2005.** Pre- and postinvasion defenses both contribute to nonhost resistance in *Arabidopsis*. *Science* **310**: 1180–1183.

**Lundberg DS, Ayutthaya PPN, Strauss A, Shirsekar G, Lo WS, Lahaye T, Weigel D. 2021.** Host-associated microbe PCR (hamPCR) enables convenient measurement of both microbial load and community composition. *eLife* **10**: e66186.

**Matsushima R, Fukao Y, Nishimura M, Hara-Nishimura I. 2004.** *NAI1* gene encodes a basic-helix-loop-helix–type putative transcription factor that regulates the formation of an endoplasmic reticulum–derived structure, the ER body. *Plant Cell* **16**: 1536–1549.

**Matsushima R, Hayashi Y, Kondo M, Shimada T, Nishimura M, Hara-Nishimura I. 2002.** An endoplasmic reticulum-derived structure that is induced under stress conditions in Arabidopsis. *Plant Physiology* **130**: 1807–1814.

**Matsushima R, Hayashi Y, Yamada K, Shimada T, Nishimura M, Hara-Nishimura I. 2003a.** The ER body, a novel endoplasmic reticulum-derived structure in Arabidopsis. *Plant and Cell Physiology* **44**: 661–666.

**Matsushima R, Kondo M, Nishimura M, Hara-Nishimura I. 2003b.** A novel ER-derived compartment, the ER body, selectively accumulates a beta-

glucosidase with an ER-retention signal in Arabidopsis. *The Plant Journal* **33**: 493–502.

Mesny F, Miyauchi S, Thiergart T, Pickel B, Atanasova L, Karlsson M, Huttel B, Barry KW, Haridas S, Chen C *et al.* **2021.** Genetic determinants of endophytism in the Arabidopsis root mycobiome. *Nature Communications* **12**: 7227.

Millet YA, Danna CH, Clay NK, Songnuan W, Simon MD, Werck-Reichhart D, Ausubel FM. **2010.** Innate immune responses activated in Arabidopsis roots by microbe-associated molecular patterns. *Plant Cell* **22**: 973–990.

Nagano AJ, Maekawa A, Nakano RT, Miyahara M, Higaki T, Kutsuna N, Hasezawa S, Hara-Nishimura I. **2009.** Quantitative analysis of ER body morphology in an *Arabidopsis* mutant. *Plant and Cell Physiology* **50**: 2015–2022.

Nakano RT, Pislewska-Bednarek M, Yamada K, Edger PP, Miyahara M, Kondo M, Bottcher C, Mori M, Nishimura M, Schulze-Lefert P *et al.* **2017.** PYK10 myrosinase reveals a functional coordination between endoplasmic reticulum bodies and glucosinolates in *Arabidopsis thaliana. The Plant Journal* **89**: 204–220.

Nakano RT, Yamada K, Bednarek P, Nishimura M, Hara-Nishimura I. **2014.** ER bodies in plants of the Brassicales order: biogenesis and association with innate immunity. *Frontiers in Plant Science* **5**: 73.

Nakazaki A, Yamada K, Kunieda T, Sugiyama R, Hirai MY, Tamura K, Hara-Nishimura I, Shimada T. **2019.** Leaf endoplasmic reticulum bodies identified in Arabidopsis rosette leaves are involved in defense against herbivory. *Plant Physiology* **179**: 1515–1524.

Nilsson RH, Larsson KH, Taylor AFS, Bengtsson-Palme J, Jeppesen TS, Schigel D, Kennedy P, Picard K, Glockner FO, Tedersoo L *et al.* **2019.** The UNITE database for molecular identification of fungi: handling dark taxa and parallel taxonomic classifications. *Nucleic Acids Research* **47**: D259–D264.

Ogasawara K, Yamada K, Christeller JT, Kondo M, Hatsugai N, Hara-Nishimura I, Nishimura M. **2009.** Constitutive and inducible ER bodies of *Arabidopsis thaliana* accumulate distinct β-glucosidases. *Plant and Cell Physiology* **50**: 480–488.

Pang Z, Chong J, Zhou G, de Lima Morais DA, Chang L, Barrette M, Gauthier C, Jacques PE, Li S, Xia J. **2021.** METABOANALYST 5.0: narrowing the gap between raw spectra and functional insights. *Nucleic Acids Research* **49**: W388–W396.

Pastorczyk M, Bednarek P. **2016.** Chapter seven – the function of glucosinolates and related metabolites in plant innate immunity. In: Kopriva S, ed. *Advances in botanical research.* Cambridge, MA, USA: Academic Press, 171–198.

Pedras MSC, Yaya EE, Glawischnig E. **2011.** The phytoalexins from cultivated and wild crucifers: chemistry and biology. *Natural Product Reports* **28**: 1381–1405.

Rufian JS, Elmore JM, Bejarano ER, Beuzon CR, Coaker GL. **2021.** ER bodies are induced by *Pseudomonas syringae* and negatively regulate immunity. *Molecular Plant–Microbe Interactions* **34**: 1001–1009.

Schreiner M, Krumbein A, Knorr D, Smetanska I. **2011.** Enhanced glucosinolates in root exudates of *Brassica rapa* ssp. *rapa* mediated by salicylic acid and methyl jasmonate. *Journal of Agricultural and Food Chemistry* **59**: 1400–1405.

Silva-Navas J, Moreno-Risueno MA, Manzano C, Pallero-Baena M, Navarro-Neila S, Tellez-Robledo B, Garcia-Mina JM, Baigorri R, Gallego FJ, del Pozo JC. **2015.** D-root: a system for cultivating plants with the roots in darkness or under different light conditions. *The Plant Journal* **84**: 244–255.

Singh G, Argawal H, Bednarek P. **2022.** Specialized metabolites as versatile tools in shaping plant-microbe associations. *Molecular Plant* **16**: 122–144.

Strehmel N, Bottcher C, Schmidt S, Scheel D. **2014.** Profiling of secondary metabolites in root exudates of *Arabidopsis thaliana. Phytochemistry* **108**: 35–46.

Stringlis IA, Yu K, Feussner K, de Jonge R, van Bentum S, Van Verk MC, Berendsen RL, Bakker PAHM, Feussner I, Pieterse CMJ. **2018.** MYB72-dependent coumarin exudation shapes root microbiome assembly to promote plant health. *Proceedings of the National Academy of Sciences, USA* **115**: E5213–E5222.

Tan JW, Bednarek P, Liu HK, Schneider B, Svatos A, Hahlbrock K. **2004.** Universally occurring phenylpropanoid and species-specific indolic metabolites in infected and uninfected *Arabidopsis thaliana* roots and leaves. *Phytochemistry* **65**: 691–699.

Tsugawa H, Cajka T, Kind T, Ma Y, Higgins B, Ikeda K, Kanazawa M, VanderGheynst J, Fiehn O, Arita M. **2015.** MS-DIAL: data-independent MS/MS deconvolution for comprehensive metabolome analysis. *Nature Methods* **12**: 523–526.

Wippel K, Tao K, Niu YL, Zgadzaj R, Kiel N, Guan R, Dahms E, Zhang PF, Jensen DB, Logemann E *et al.* **2021.** Host preference and invasiveness of commensal bacteria in the Lotus and Arabidopsis root microbiota. *Nature Microbiology* **6**: 1150–1162.

Wittstock U, Halkier BA. **2002.** Glucosinolate research in the Arabidopsis era. *Trends in Plant Science* **7**: 263–270.

Wolinska KW, Vannier N, Thiergart T, Pickel B, Gremmen S, Piasecka A, Pislewska-Bednarek M, Nakano RT, Belkhadir Y, Bednarek P *et al.* **2021.** Tryptophan metabolism and bacterial commensals prevent fungal dysbiosis in Arabidopsis roots. *Proceedings of the National Academy of Sciences, USA* **118**: e2111521118.

Xu DY, Hanschen FS, Witzel K, Nintemann SJ, Nour-Eldin HH, Schreiner M, Halkier BA. **2017.** Rhizosecretion of stele-synthesized glucosinolates and their catabolites requires GTR-mediated import in Arabidopsis. *Journal of Experimental Botany* **68**: 3205–3214.

Yamada K, Goto-Yamada S, Nakazaki A, Kunieda T, Kuwata K, Nagano AJ, Nishimura M, Hara-Nishimura I. **2020.** Endoplasmic reticulum-derived bodies enable a single-cell chemical defense in Brassicaceae plants. *Communications Biology* **3**: 21.

Zhang P, Spaepen S, Bai Y, Hacquard S, Garrido-Oter R. **2021.** Rbec: a tool for analysis of amplicon sequencing data from synthetic microbial communities. *ISME Communications* **1**: 73.

Zhao YD, Hull AK, Gupta NR, Goss KA, Alonso J, Ecker JR, Normanly J, Chory J, Celenza JL. **2002.** Trp-dependent auxin biosynthesis in Arabidopsis: involvement of cytochrome P450s CYP79B2 and CYP79B3. *Genes & Development* **16**: 3100–3112.

## Supporting Information

Additional Supporting Information may be found online in the Supporting Information section at the end of the article.

**Fig. S1** Community shifts observed in the mutant roots compared with Col-0 roots retained at the family level.

**Fig. S2** Multiple amplicon sequence variants represent top-abundant families.

**Fig. S3** Similar effects of endoplasmic reticulum body pathway and Trp metabolism on root microbiota community structure at the amplicon sequence variant level.

**Fig. S4** Similar effects of endoplasmic reticulum body pathway and Trp metabolism on root microbiota community structure at the family level.

**Fig. S5** Several bacterial and fungal families are commonly enriched or depleted in mutant roots compared with wild-type roots.

**Fig. S6** Relative amounts of glucosinolates, selected Trp derivatives, and coumarins in the mutant root exudates and extracts.

**Fig. S7** Community dynamics and growth of individual microbes in a SynCom treated with root exudates.

**Table S1** List of bacterial strains used in the SynCom.

**Table S2** List of fungal strains used in the mono-association assay.

**Table S3** Barcoded primers used for bacterial 16S V5–V7 amplicon sequencing.

**Table S4** Barcoded primers used for bacterial ITS1 amplicon sequencing.

**Table S5** Forward barcoded primer set for bacterial 16S V5–V7 amplicon sequencing.

**Table S6** Forward barcoded primer set for bacterial ITS1 amplicon sequencing.

**Table S7** Summary statistics of community structure analysis by constrained ordination followed by pairwise PERMANOVA for the glasshouse experiment.

**Table S8** List of targeted compounds quantified in root exudates.

**Table S9** Summary statistics of community structure analysis by constrained ordination followed by pairwise PERMANOVA for the soil treatment experiment.

**Table S10** Summary statistics of community structure analysis by constrained ordination followed by pairwise PERMANOVA for the SynCom experiment.

Please note: Wiley is not responsible for the content or functionality of any Supporting Information supplied by the authors. Any queries (other than missing material) should be directed to the *New Phytologist* Central Office.